Searching for Magnetism in Hydrogenated Graphene: Using Highly Hydrogenated Graphene Prepared *via* Birch Reduction of Graphite Oxides

Alex Yong Sheng Eng,[†] Hwee Ling Poh,[†] Filip Šaněk,[‡] Miroslav Maryško,[§] Stanislava Matějková,[⊥] Zdeněk Sofer,[‡,*] and Martin Pumera[†,*]

[†]Division of Chemistry & Biological Chemistry, School of Physical and Mathematical Sciences, Nanyang Technological University, Singapore 637371, Singapore, [‡]Institute of Chemical Technology, Department of Inorganic Chemistry, 166 28 Prague 6, Czech Republic, [§]Institute of Physics of the AS CR, v.v.i., Cukrovarnická 10/112, 162 00 Prague 6, Czech Republic, and [⊥]Institute of Organic Chemistry and Biochemistry AS CR, v.v.i., Flemingovo nám. 2., 166 10 Praha 6, Czech Republic

ABSTRACT Fully hydrogenated graphene (graphane) and partially hydrogenated graphene materials are expected to possess various fundamentally different properties from graphene. We have prepared highly hydrogenated graphene containing 5% wt of hydrogen *via* Birch reduction of graphite oxide using elemental sodium in liquid NH_3 as electron donor and methanol as proton donor in the reduction. We also investigate the influence of preparation method of graphite oxide, such as the Staudenmaier, Hofmann or Hummers methods on the hydrogenation rate. A control experiment involving $NaNH_2$ instead of elemental Na was also performed. The materials were characterized in detail by electron microscopy, infrared spectroscopy, X-ray photoelectron spectroscopy, Raman spectroscopy both at room and low temperatures, X-ray fluorescence spectroscopy, inductively coupled plasma optical emission spectroscopy, combustible elemental analysis and electrical resistivity measurements. Magnetic measurements are provided of bulk quantities of highly hydrogenated graphene. In the whole temperature range up to room temperature, the hydrogenated graphene exhibits a weak ferromagnetism in addition to a contribution proportional to field that is caused not only by diamagnetism but also likely by an antiferromagnetic influence. The origin of the magnetism is also determined to arise from the hydrogenated graphene itself, and not as a result of any metallic impurities.

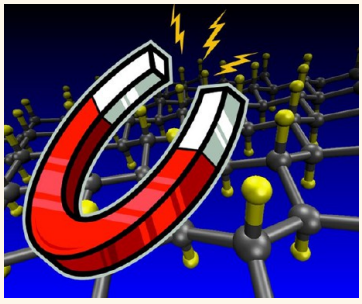

KEYWORDS: hydrogenated graphene · graphane · graphite oxide · ferromagnetism

Graphane, the fully hydrogenated derivative of graphene with theoretical composition $(C_1H_1)_n$, was hypothesized by several authors.[1,2] Partially and fully hydrogenated graphenes are proposed to have a myriad of fascinating properties that include a tunable band gap,[3−7] and also exhibit fluorescence[8] and ferromagnetism.[9] Numerous attempts to prepare partially hydrogenated graphene have been focused on two strategies: (i) gas phase hydrogenation of graphene[10−15] and (ii) liquid phase hydrogenation/exfoliation of graphite.[8,16,17] The first approach using H_2 gas to hydrogenate graphene at various temperature and pressure leads to <10% partial hydrogenation of graphene.[11,14] In contrast, wet chemistry hydrogenation employs the Birch reduction of aromatic rings using solutions of solvated electrons, by first dissolving Li or Na in liquid NH_3 with consequent provision of protons *via* use of alcohols. Such a reduction can produce hydrogenated graphene with composition of $(C_{1.3}H_1)_n$ and is thus more successful than gas-phase hydrogenation.[17] Nonetheless in all cases represented in the literature, only partially hydrogenated graphene was prepared, and fully hydrogenated graphane still remains elusive. Interestingly though, the controllable properties of hydrogenated graphenes may be of even greater significance that the ones of pure graphane. Of particular interest is the ferromagnetism which may be found in partially hydrogenated graphene,[14] and which is entirely absent in pristine graphene[18] and fully hydrogenated graphane.[4] Both these materials represent the extremes of the hydrogenation extent, and have been shown to be strongly nonferromagnetic.[19] Weak paramagnetism was only detectable in graphene at very low temperatures of below 50 K and only as a result of a minute amount of defects.[18,20] In contrast, there exists an

* Address correspondence to pumera@ntu.edu.sg.

Received for review April 2, 2013 and accepted June 11, 2013.

Published online June 18, 2013
10.1021/nn4016289

abundance of experimental studies on the room-temperature paramagnetism and even ferromagnetism of fluorinated graphene,[21] defective graphene sheets,[20,22] aryl-functionalized graphene,[23] reduced-graphene oxides at temperatures close to 10 K,[24] and also theoretical studies on ferromagnetism of partially hydrogenated graphene.[9,19,25] Here, we provide experimental investigation into magnetism originating from the bulk quantities of highly hydrogenated graphene. Collectively, defects, vacancies, residual oxygen moieties and adsorbed atoms have all been proposed to give rise to localized magnetic moments that result in their observed magnetism.

Therefore, toward this end, the use of graphite oxide (GO) as starting material[26] presents interesting prospects, and there are multiple motives in our use of the Birch reduction technique on GO to fabricate hydrogenated graphene. Clearly, our primary aim in using the Birch reduction is to achieve hydrogenation of the sp^2-carbon lattice. However, the structure of graphite oxide is intrinsically imperfect,[27] containing a multitude of oxygen functionalities along with sporadic defects created by the harsh conditions during its oxidation from graphite. An additional purpose, thus, is that the reducing nature of the Birch procedure (sodium dissolved in liquid ammonia) may also serve in the removal of some oxygen-containing groups,[28] bypassing the need for a prior reduction step.[29] In this article, we systematically evaluate the suitability of graphene oxides prepared by various standard methods (namely, the Staudenmaier,[30] Hofmann[31] and Hummers[32] methods) to undergo Birch reduction using Na as an electron donor and methanol as a proton donor.[33] We present our findings on the nature of Birch-reduced graphene oxides, with extensive characterization by scanning electron microscopy (SEM), energy-dispersive X-ray spectroscopy (EDS), Fourier-transform infrared spectroscopy (FTIR), X-ray photoelectron spectroscopy (XPS), combustible elemental analysis, energy-dispersive X-ray fluorescence spectroscopy (ED-XRF), inductively coupled plasma optical emission spectroscopy (ICP-OES), Raman spectroscopy, photoluminescence measurements and electrical resistivity measurements. The magnetic properties of the hydrogenated graphenes were investigated with superconducting quantum interference device (SQUID) magnetometry.

RESULTS AND DISCUSSION

In this paper, we employ the Birch technique in the simultaneous reduction and hydrogen functionalization of graphite oxides. Three types of graphite oxide are first prepared using the Staudenmaier ($KClO_3$ in concentrated H_2SO_4 and fuming HNO_3),[30] Hofmann ($KClO_3$ in concentrated H_2SO_4 and HNO_3)[31] and Hummers ($KMnO_4$ in concentrated H_2SO_4 and $NaNO_3$)[32] methods. These are subsequently treated with sodium in liquid ammonia to yield the hydrogenated graphenes. In addition, a fourth reduced-GO sample was prepared from the Hofmann method but was exposed to sodium amide in liquid ammonia ($NaNH_2/NH_{3(l)}$) for use as a comparison. We abbreviate our reduced-GOs in this paper as G-ST, G-HO, G-HU and G-HO-Control. Extensive materials characterization comprising scanning electron microscopy (SEM), energy-dispersive X-ray spectroscopy (EDS), energy-dispersive X-ray fluorescence spectroscopy (ED-XRF), inductive coupled plasma optical emission spectroscopy (ICP-OES), Fourier-transform infrared spectroscopy (FTIR), X-ray photoelectron spectroscopy (XPS), combustible elemental analysis, Raman spectroscopy, photoluminescence spectroscopy and electrical resistivity measurements were performed to elucidate the nature of resulting Birch reduced graphite oxides. Finally, magnetism measurements were conducted using a superconducting quantum interference device (SQUID).

SEM images of the four reduced-GOs were first obtained at various magnifications and these are as illustrated in Figure 1. All samples exhibit the characteristic crumpled texture of chemically reduced graphenes,[34] and have relatively uniform particle sizes. An exception is that of G-HU that shows particles with a large size distribution, which is particularly evident at low magnification. In addition, both reduced forms of the chlorate-oxidized GOs (namely, G-ST and G-HO) have a thin sheet-like appearance, while G-HU and G-HO-Control show a larger extent of wrinkling that is obvious at higher magnifications.

With the aim of determining if the hydrogenation of GOs by the Birch reduction is successful, we subsequently employ FTIR spectroscopy (Figure 2) to identify the presence of chemically bonded hydrogen. The detail spectra of C−H vibrations are shown in the Supporting Information (Figure S1). The two bands at 2850 and 2950 cm^{-1} corresponding to C−H stretches provide definitive proof of a successful hydrogenation.[8,16,17] Additionally, a number of other peaks expected of oxygen-containing groups in GO are present; a broad absorption band from 3300 to 3500 cm^{-1} corresponds to O−H vibrations from hydroxyl and carboxyl groups, a peak at *ca.* 1650 cm^{-1} due to C═O stretching, a band at 1580 cm^{-1} due to aromatic C═C stretching and also a set of complex bands between 1000 and 1300 cm^{-1} arising from multiple C−C and C−O vibrations.[35,36] Although these observations indicate a continued presence of oxygen functionalities within all reduced-GOs, it should be noted that no single GO reduction procedure has been shown to completely remove all its inherent oxygen moieties.[37]

To further elucidate the oxygen contents and functionalities of the Birch-reduced-GOs, X-ray photoelectron spectroscopy is used in obtaining both the elemental and chemical surface compositions.[38] Figure 3 shows the survey spectra of the reduced-GO samples

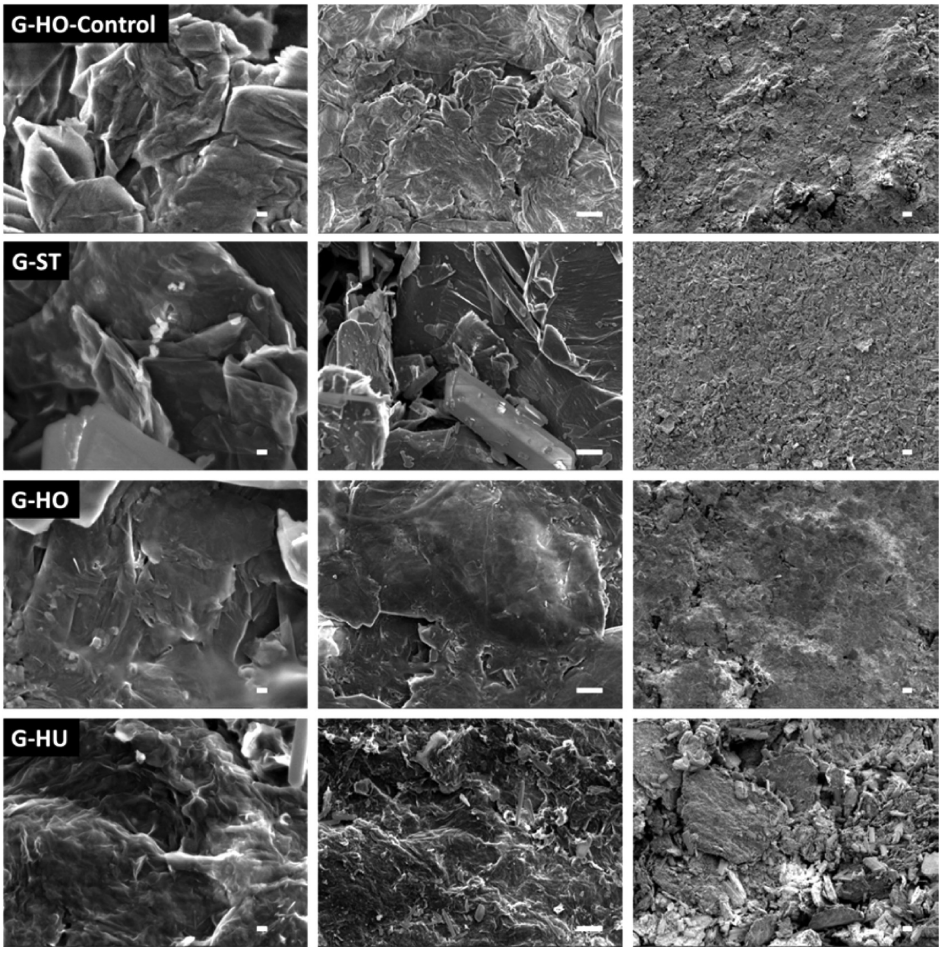

Figure 1. Scanning electron micrographs of hydrogenated graphenes prepared from graphite oxides synthesized by the Staudenmaier (G-ST), Hofmann (G-HO) and Hummers (G-HU) methods with subsequent Birch reduction in Na/NH_3 and methanol. Also shown are the electron micrographs of the control experiment, where Hofmann graphite oxide was treated by $NaNH_2/NH_3$ (G-HO Control). Scale bars are 100 nm, 1 μm, and 10 μm, respectively.

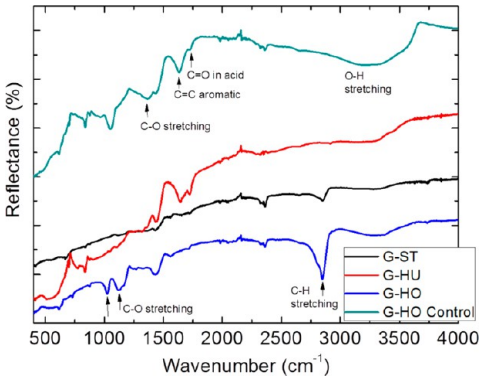

Figure 2. FT-IR spectra of hydrogenated graphenes prepared from graphite oxides synthesized by the Staudenmaier (G-ST), Hofmann (G-HO) and Hummers (G-HU) methods with subsequent Birch reduction in Na/NH_3 and methanol. Also shown is the FT-IR spectra of our control experiment, where Hofmann graphite oxide was treated by $NaNH_2/NH_3$ (G-HO Control).

and their surface atomic compositions are tabulated in Table 1. Three prominent peaks corresponding to electrons from the core-level carbon-1s, oxygen-1s and sodium-1s orbitals are apparent at binding energies of *ca.* 285, 534, and 1070 eV respectively. In some cases, a small signal at 165 eV corresponding to the sulfur-2p orbital is also observed due to the use of sulfuric acid in the oxidation procedure of graphite. In evaluating the reducing ability of the Birch procedure on oxygen-containing groups in GO, we use the ratio of peak intensities of the carbon-1s *versus* the oxygen-1s core levels (denoted C/O ratio) as a measure of the degree of remaining oxygen functionalities. Large C/O ratios are indicative of successful reductions of graphite oxides. The largest ratio was calculated to be 8.79 for G-HO as reduced by the Birch process; in comparison to 2.78 for a control we performed with the same material using sodium amide in liquid ammonia. Interestingly, the procedure exhibits varying reducing abilities on different GOs, with a lower ratio of 5.53 for G-ST and a significantly low value of 2.25 for G-HU. As a comparison, C/O ratios of unreduced GOs are 2.47, 2.71, and 2.05 for GO-ST, GO-HO, and GO-HU, respectively.[39] A similar trend is noted with energy-dispersive X-ray spectroscopic data in the Supporting Information (Table S1), with G-HO having the highest carbon content relative to oxygen, followed by G-ST, G-HO-Control and

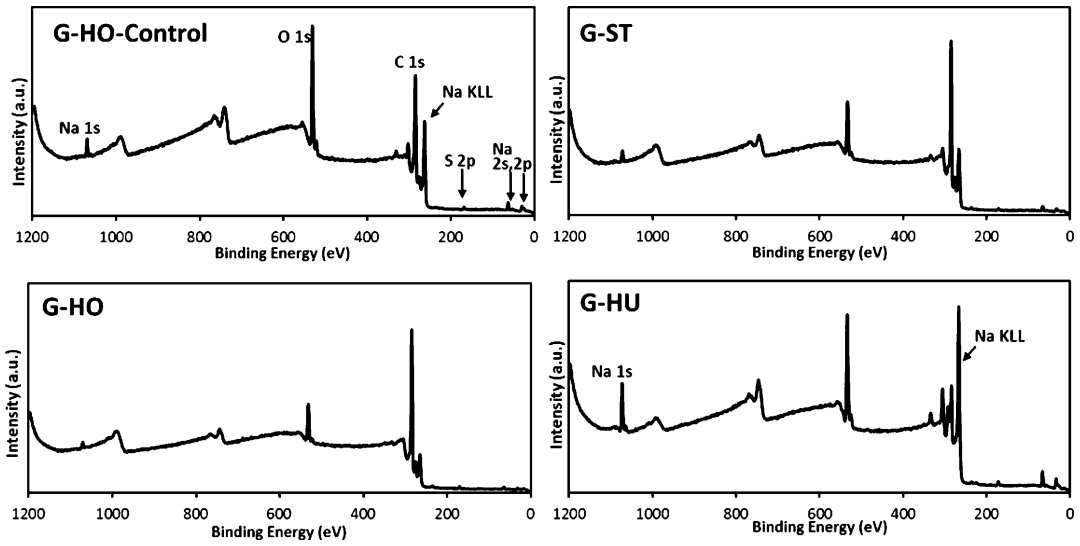

Figure 3. Wide-scan XPS spectra of hydrogenated graphenes prepared from graphite oxides synthesized by the Staudenmaier (G-ST), Hofmann (G-HO) and Hummers (G-HU) methods with subsequent Birch reduction in Na/NH_3 and methanol. Also shown is XPS spectra of the control experiment, where Hofmann graphite oxide was treated by $NaNH_2/NH_3$ (G-HO Control).

TABLE 1. Wide Scan XPS Quantitative Comparison of Composition of Various Hydrogenated Graphenes Prepared from Graphite Oxides

		atomic percentages			
material[a]	C/O ratio	carbon-1s (285 eV)	oxygen-1s (534 eV)	sodium-1s (1070 eV)	sulfur-2p (165 eV)
G-HO-Control	2.78	71.96	25.84	1.56	0.64
G-ST	5.53	83.49	15.10	1.41	Not detected
G-HO	8.79	88.62	10.08	0.55	0.75
G-HU	2.25	64.17	28.55	5.71	1.56

[a] Graphite oxides are synthesized by Staudenmaier (G-ST), Hofmann (G-HO) and Hummers (G-HU) methods with subsequent Birch reduction in Na/NH_3 and methanol. Also shown is the elemental composition of control experiment, where Hofmann graphite oxide was treated by $NaNH_2/NH_3$ (G-HO Control).

finally G-HU. Hence, the Birch procedure is most effective for G-HO but has a practically negligible effect on the removal of oxygen groups in G-HU. It is also seen from XPS that a variable amount of sodium is introduced into the reduced graphenes, from 0.55% in G-HO up to 5.71% in G-HU. This observation is in agreement with previous reports utilizing a similar Birch hydrogenation process with lithium metal, suggesting a similar event of sodium-intercalation into graphene for our current study.[8,17,28] In addition, a set of peaks due to Auger electrons arising from KLL transitions in sodium are observed at binding energies of 264, 301 and 331 eV. These observations corroborate with evidence from our EDS mappings in Figure S2, where we also find the presence of Na, specifically at carbon-rich sites and typically less abundant at oxygen-rich areas. The sodium content in the various reduced graphenes from EDS (Table S1) showed a similar trend with XPS as seen in Table 1.

TABLE 2. Elemental Analysis (atomic %) of Hydrogenated Graphenes Based on Combustible Analysis[a]

material	N (atom %)	C (atom %)	S (atom %)	H (atom %)	O (atom %)
G-HO-Control	0.28	36.35	0	25.72	37.65
G-ST	0.32	57.99	0	25.06	16.63
G-HO	0.38	51.79	0	37.42	10.41
G-HU	0.21	54.3	0	11.42	34.07

[a] Data for various hydrogenated graphenes prepared from graphite oxides synthesized by Staudenmaier (G-ST), Hofmann (G-HO) and Hummers (G-HU) methods with subsequent Birch reduction in Na/NH_3 and methanol are shown. Also shown is the elemental composition of our control material, where Hofmann graphite oxide was treated by $NaNH_2/NH_3$ (G-HO Control). Corresponding table for wt % can be found in the Supporting Information.

Thus far, infrared spectroscopy and X-ray photoelectron spectroscopy have independently provided definitive proof of successful hydrogenation and also of the removal of oxygen groups. However, both techniques do not provide quantification of the absolute extents of hydrogenation or the amount of remaining oxygen. Therefore, the use of combustible elemental analysis was executed to achieve both these objectives. As seen from Table 2, the amount of hydrogen introduced was as high as 37.42 atom % in G-HO (4.54 wt %), comparable to the highest reported hydrogenation extent of 5 wt % as obtained by Rao.[16] The level of hydrogenation then decreases to 2.55% by weight for G-ST, 2.43% for G-HO-Control and only 0.95% for G-HU (Table S2). The trend observed for the oxygen content is roughly the opposite, decreasing in the order: G-HO-Control > G-HU > G-ST > G-HO. If we express the composition of hydrogenated graphenes by general formula, we find that G-ST consists of $C_{2.31}H_1O_{0.66}$; G-HO $C_{1.38}H_1O_{0.28}$; G-HU $C_{4.75}H_1O_{2.98}$, while control sample G-HO-Control consists of $C_{1.41}H_1O_{1.47}$. It is clear that for G-HO-Control as well as for G-HU, there is a larger content of O in

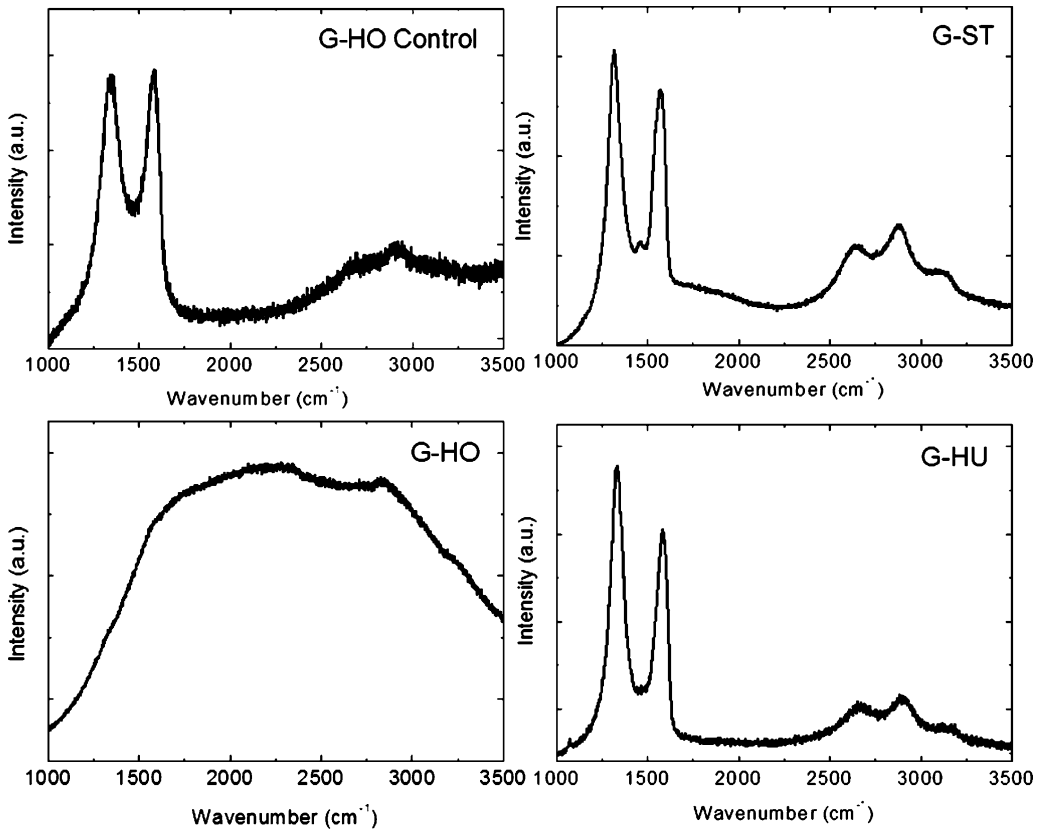

Figure 4. Raman spectra of hydrogenated graphenes prepared from graphite oxides synthesized by the Staudenmaier (G-ST), Hofmann (G-HO) and Hummers (G-HU) methods with subsequent Birch reduction in Na/NH_3 and methanol. Also shown is the Raman spectra of the control experiment, where Hofmann graphite oxide was treated by $NaNH_2/NH_3$ (G-HO Control).

comparison to H, and therefore, it cannot be ruled out that most H atoms are bonded to O atoms as hydroxyl or carboxyl groups. However, G-ST and G-HO exhibit larger amounts of H than O; in addition, G-HO shows a remarkable C:H ratio of 1.38:1. Thus, these demonstrate that hydrogenation of the carbon backbone itself was highly successful, such that the vast majority of hydrogen atoms are carbon-bonded and not oxygen-bonded in the case of G-HU and G-HO-Control. It is also interesting to observe that minute amounts of nitrogen on the samples were detected, presumably from the use of nitric acid in the oxidation of graphite. The highest nitrogen concentration of only 0.64 wt % was obtained for the most hydrogenated G-HO material (Table S2).

To investigate the structural properties, Raman and photoluminescence spectroscopy were employed. The samples with lower hydrogen contents exhibit spectra typical of graphene materials. These spectra are dominated by the D band (1350 cm^{-1}) and G band (1560 cm^{-1}) which represent defects in the sp^2 lattice, and the vibrations in pristine graphene layers respectively. The density of defects can be compared between the various materials by calculation of the relative D to G band intensities, with higher ratios indicating increased disorder in the graphene structure. In the spectra, we may also find broad peaks related to the 2D phonon mode (located around 2650 cm^{-1}) and the D+D' phonon mode (located around 2880 cm^{-1}). Figure 4 shows the Raman spectra of graphene treated with Na/NH_3 and $NaNH_2/NH_3$. For the measurement, a low laser power of 500 μW was used in order to avoid overheating and damage to the sample. The I_D/I_G ratio was 1.32 for the G-HU sample and 1.30 for G-ST (Table 3). In comparison, the G-HO-Control sample has a considerably lower I_D/I_G ratio of 1.00. The high I_D/I_G ratio is directly related to the synthesis procedure which involves the intercalation of sodium solution inside the GO layers with subsequent hydrogenation and exfoliation by the reaction with methanol acting as proton donor. Thus, it indicates the formation of sp^3 carbon atoms with covalently bonded hydrogen on the graphene basal plane. In addition, the average crystallite size (L_a) can also be directly calculated using the reciprocal of the I_D/I_G ratio based on eq (1):[40]

$$L_a = 2.4 \times 10^{-10} \times \lambda_{laser}{}^4 \times I_G/I_D \qquad (1)$$

The I_G/I_D is the ratio of the intensities of the G and D bands, respectively, and λ_{laser} refers to the laser wavelength (nm) used in the measurement of the Raman spectrum, *i.e.*, 532 nm. The values obtained for the G-HU are 14.6 and 14.8 nm for G-ST. The crystallite size of G-HO-Control sample is 19.2 nm. These observations

TABLE 3. D to G Band Intensity Ratios and Crystallite Sizes (L_a) of Hydrogenated Graphenes Based on Raman Spectroscopy

material	I_D/I_G ratio	L_a (nm)
G-HO-Control	1.00	19.2
G-ST	1.30	14.8
G-HO[a]	0.98	19.6
G-HU	1.32	14.6

[a] Measurement of G-HO performed at 11 K; all other materials at room temperature.

suggest that the process of reduction/hydrogenation is accompanied with decrease of crystallite size as a result of the violent reaction of intercalated sodium with methanol.

In contrast to the other samples (G-ST, G-HU and G-HO-Control), the high degree of hydrogenation in the case of G-HO led to complete overlap of D and G peaks due to strong photoluminescence of the sample. The presence of photoluminescence may be attributed to band gap splitting by the covalently bonded hydrogen in graphane. Graphane has been predicted by *ab initio* calculation to exhibit behavior resembling direct band gap semiconductors with the E_g level dependent on the degree of hydrogenation,[41] and strong photoluminescence was reported for graphene with high hydrogen content.[8] To obtain Raman spectra from the G-HO sample with strong luminescence intensity, low temperature Raman spectra and FT Raman spectra with 1064 nm infrared laser were measured. FT-Raman spectroscopy (Figure S3) did not provide useful results due to the low intensity of G and D phonon modes excited with IR laser, and the strong photoluminescence background was again observed even in the IR region. On the basis of these results, low temperature Raman spectroscopy was performed on the highly hydrogenated G-HO sample. With the sample placed inside a cryostat, we used a Vis-NIR optimized long working distance objective with 20× magnification for the purposes of laser focusing and signal collection. The temperature reduction led to enhancement of both D and G phonon mode intensities and below 100 K they can be clearly observed. The I_D/I_G ratio of 0.98 was found at 11 K. This value was calculated with subtraction of the photoluminescence baseline and is comparable with the I_D/I_G ratio obtained for the control sample measured at room temperature. The corresponding crystallite size calculated was 19.6 nm. The temperature dependence of the peak intensities for the G-HO sample was investigated both with a laser power of 500 μW as shown in Figure 5, and also at 50 μW (Figure S4). The reduction of laser power led to further decrease of background photoluminescence intensities, however the signal-to-noise ratio is also lower.

As a result of the strong photoluminescence background from G-HO, we proceed with further measurements of

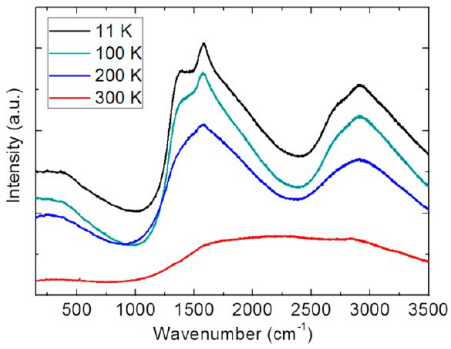

Figure 5. Temperature dependence of Raman spectra measured on hydrogenated graphenes (G-HO) prepared according to the Hofmann method and reduced with Na/NH_3 and methanol.

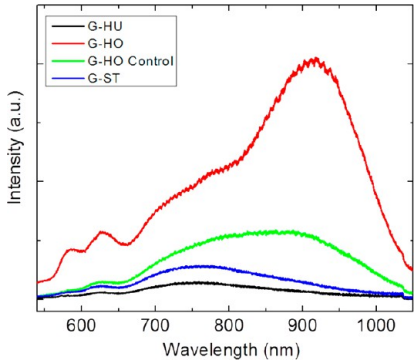

Figure 6. Photoluminescence spectra of hydrogenated graphenes prepared from graphite oxides synthesized by Staudenmaier (G-ST), Hofmann (G-HO) and Hummers (G-HU) methods with following Birch reduction in Na/NH_3 and methanol. Also shown is the photoluminescence spectra of the control experiment, where Hofmann graphite oxide was treated by $NaNH_2$/NH_3 (G-HO Control).

photoluminescence spectra of all samples as illustrated in Figure 6. Both G-HU and G-ST exhibit only very weak photoluminescence with maxima located around 750 nm. A slightly higher intensity was observed for the G-HO-Control sample together with a bathochromic shift. In contrast, the luminescence of G-HO was 2 orders of magnitude stronger with the maximum intensity located in the NIR region around 930 nm. A second weaker luminescence band was located at a similar position as the other materials. Presence of such strong luminescence in both the visible and NIR regions suggest formation of high concentrations of deep levels inside the band gap, and these deep levels can form the traps for free electrons. This effect is consequently documented by measurement of the materials' resistivity, where hydrogenation increases the resistivity by breaking the π-conjugation of graphene. The sample with lowest degree of hydrogenation (G-HU) has a low specific resistivity of 0.18 Ω·cm. Materials with higher hydrogen concentrations such as G-ST and G-HO have the values of 9.1 and 8.2 Ω·cm, respectively. However, a secondary influence is the presence of oxygen-containing functionalities. In addition to chemisorbed H-atoms, these

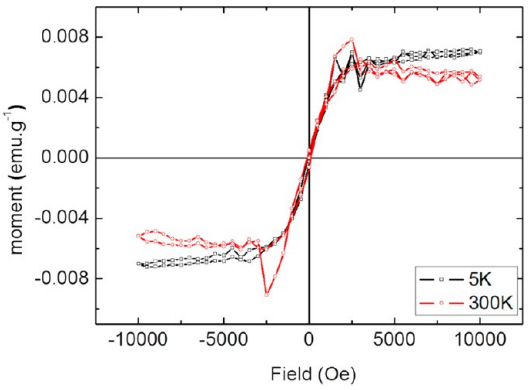

Figure 7. Magnetization measurements of hydrogenated graphene (G-HO) at 5 and 300 K.

groups also lead to the formation of deep levels and a strong electron-trapping effect. This is particularly evident in G-HO-Control which has a minimal degree of reduction and a resistivity in the order of kΩ·cm. Nonetheless, for the highly hydrogenated G-HO with its minimal oxygen content, the principal cause of the observed luminescence is due to the abundant presence of C−H bonds where the radiative recombinations take place.

Lastly, we measure the magnetic properties of the hydrogenated graphene with the highest degree of hydrogenation (G-HO) using a superconducting quantum interference device (SQUID). The hysteresis loops at T = 5 and 300 K shown in Figure 7 point to a ferromagnetic (FM) state at both these temperatures with a nearly temperature-independent ferromagnetic saturated moment 6×10^{-3} emu·g^{-1}. The temperature dependences of the zero field cooling (ZFC) and field cooling (FC) susceptibilities measured under an applied field of 1000 Oe exhibit a constant value of *ca.* 6×10^{-6} emu·g^{-1}·Oe^{-1} with a small increase at the lowest temperatures. The narrow hysteresis loop characterized by a coercivity about 100 Oe at T = 5 and 300 K suggests a soft magnetic character of G-HO. In this case, a relatively small magnetic field of 2500 Oe is sufficient for the magnetic saturation of the sample. It should be noted that this behavior is usually observed for ferromagnetic nanoparticles like iron, cobalt and nickel. In addition to the FM contribution, the hysteresis loop at T = 300 K shows a linear contribution, with respect to the magnetic field, for which the corresponding negative susceptibility can be estimated to be -8×10^{-8} emu/(g·Oe). It is interesting that the absolute value of this susceptibility is almost an order of magnitude less that the typical diamagnetic susceptibility of carbon (diamond at -4.9×10^{-7}, graphite at -5×10^{-7} across the *c*-axes and -30×10^{-6} along the *c*-axis, C_{60} at -3.5×10^{-7}, and C_{70} at -5.9×10^{-7} emu/(g·Oe)).[42] This fact could be explained if we admitted the presence of a small intrinsic antiferromagnetic (AFM) contribution (the presence of AFM impurities in G-HO is not probable), where a positive linear m(H) moment might compensate a negative m(H) contribution caused by the intrinsic diamagnetic susceptibility of carbon.

TABLE 4. Trace Analysis of Impurities in Hydrogenated Graphene G-HO As Determined by ICP-OES

element	V	Cr	Mn	Fe	Co	Ni	Al	B	Ca	Mg	Pb	In	Ti	Zr	Cd	Na
Concentration (ppm)	2	5	0	20	7	3	2	15	530	3	42	30	7	2	6	33800

The principal question therefore is whether the observed FM contribution of 6×10^{-3} emu·g^{-1} arises intrinsically from the hydrogenated graphene or if it could be caused by Fe or other impurities. An Fe impurity content of 1 μg g^{-1} would give the magnetization of 2.2×10^{-4} emu·g^{-1}.[43] The observed FM magnetization for our sample would have to correspond to 27.2 ppm of elemental iron (or 200 ppm Ni and 75 ppm Co). Hence, in order to determine the true concentration of metallic impurities and resolve the origin of ferromagnetism, trace analyses of metallic impurities in our sample were carried out. Measurements by ED-XRF with typical detection limits in range from 1 to 10 ppm for transition metals did not show any metallic impurity such as Fe, Co, Ni or any other transition metal. Further measurements using the highly sensitive technique of ICP-OES were also performed, and the concentrations of transition metals are summarized in Table 4. The total concentration of all ferromagnetic impurities (Fe, Co and Ni) is minute, and insufficient to give rise to the magnetic moment observed for the G-HO hydrogenated graphene. Another consideration that further challenges the argument that the observed magnetism could arise from metallic impurities is that these metals are unlikely to even exist in their elemental forms due to their high reactivity and affinity to atmospheric oxygen. Of the oxides, only Fe_3O_4 can have ferromagnetic behavior, and its saturated magnetic moment is much weaker compared to elemental iron.

Hence, it can be stated here that the observed FM contribution in hydrogenated G-HO appears to be of an intrinsic nature, and there is also an indication of the presence of an intrinsic AFM contribution with Néel temperature above 300 K. We attribute the magnetic ordering (ferromagnetism) in G-HO primarily to its large extent of hydrogenation, with strong theoretical evidence[9,19] in support of this proposition. In addition to the ferromagnetism, multiple defects in the material also render a smaller observed antiferromagnetic contribution, as seen from computational methods.[44]

CONCLUSION

We demonstrate for the first time that the Birch reduction of graphite oxides can lead to highly hydrogenated graphene of composition $C_{1.38}H_1O_{0.28}$. We also investigated

the Birch reduction procedure on graphite oxides prepared by several methods, and report a dramatic variation in the success of the simultaneous reduction and hydrogenation procedure on these substrates. Extensive characterization was performed on the highly hydrogenated graphenes and we studied the magnetic properties of the hydrogenated graphene. Here, we show the experimental evidence of their magnetism and its intrinsically complex nature, consisting of both ferromagnetic and antiferromagnetic components.

METHODS

Materials. Sulfuric acid (98%, p.a.), nitric acid (68%, p.a.), potassium chlorate (99%, p.a.), potassium permanganate (99.5%, p.a.), hydrogen peroxide (30%, p.a.), hydrochloric acid (35%, p.a.) were obtained from PENTA, Czech Republic. Graphite microparticles (2−15 μm, 99.9995% purity) were obtained from Alfa Aesar. Ammonia (99.999%) and argon (99.996%) were purchased from SIAD. Sodium (99.8%), sodium amide (98%), and methanol (99.9%) were obtained from Sigma-Aldrich. Deionized water with a resistivity of 18.2 MΩ · cm was used throughout in the preparation of solutions.

Synthetic Procedures. *Synthetic Procedure of Staudenmaier Graphite Oxide*[30]. The synthesis of GO-ST was performed according to the procedure reported previously. A total of 87.5 mL of sulfuric acid (98%) and 27 mL of fuming nitric acid (98%) were first cooled to 0 °C before 5 g of graphite was added to the mixture. The reaction mixture was then intensively stirred while 55 g of potassium chlorate was added over a period of 30 min. The reaction flask was then loosely capped to allow the escape of chlorine dioxide gas. The mixture was continuously stirred for 96 h at room temperature and then poured into 3 L of deionized water. After decantation, the graphite oxide was redispersed in 5% hydrochloric acid. The graphite oxide was again decanted from the hydrochloric acid and repeatedly centrifuged and redispersed until a negative reaction for chloride and sulfate ions (with $Ba(NO_3)_2$ and $AgNO_3$) was observed. Graphite oxide slurry was finally dried in a vacuum oven at 60 °C for 48 h before further use.

Synthetic Procedure of Hofmann Graphite Oxide[31]. The synthesis of GO-HO was performed according to the standard method reported in literature. A total of 87.5 mL of concentrated sulfuric acid (98%) and 27 mL of nitric acid (68%) were first cooled to 0 °C before 5 g of graphite was dispersed into the reaction mixture by vigorous stirring. Keeping the reaction mixture vigorously stirred at 0 °C, $KClO_3$ (55 g) was then added over a period of 30 min. The reaction mixture was loosely capped to allow the escape of gaseous reaction products (ClO_2) and stirred at room temperature for 96 h. Upon completion of reaction, the mixture was poured into 3 L of deionized water and decanted. The reaction product was then redispersed in 2 L of 5% HCl and decanted. Graphite oxide was then repeatedly centrifuged and redispersed in deionized water until a negative reaction on sulfate and chloride ions (with $Ba(NO_3)_2$ and $AgNO_3$, respectively) was achieved. Graphite oxide slurry was finally dried in a vacuum oven at 60 °C for 48 h before subsequent use.

Synthetic Procedure of Hummers Graphite Oxide[32]. The synthesis of GO-HU was performed according to the method reported previously. A total of 115 mL of sulfuric acid (98%) was cooled to 0 °C and then 5 g of graphite and 2.5 g of $NaNO_3$ were added to the mixture. While vigorously stirred, 15 g of $KMnO_4$ was added over a period of 2 h. The reaction mixture was then removed from the cooling bath and stirred at room temperature for 4 h. The reaction mixture was then heated to 35 °C for 30 min, poured into 250 mL of deionized water and heated to 70 °C. After 15 min the mixture was poured into 1 L of deionized water. Unreacted $KMnO_4$ was decomposed with 10% hydrogen peroxide. The reaction mixture was then decanted and repeatedly centrifuged and redispersed until a negative reaction for sulfate ions (with $Ba(NO_3)_2$) was achieved. Graphite oxide slurry was then dried in a vacuum oven at 60 °C for 48 h before further use.

Reduction of Graphite Oxide with Sodium in Liquid Ammonia (Birch Reduction). The reduction of GO with sodium in liquid ammonia was performed under argon atmosphere. For the cooling of the reflux condenser, a dry ice acetone mixture was used. The 60 mL of ammonia was condensed in 250 mL flask equipped with magnetic stirring. Then, 60 mg of each GO was added to the liquid ammonia and stirred for 10 min. The flask with liquid ammonia was held at −30 °C. Subsequently, 1 g of sodium was added to the reaction mixture and the temperature was increased to −15 °C to start reflux of ammonia. After 2 h, 30 mL of methanol was added. After addition of methanol, the reaction mixture was allowed to warm to room temperature overnight. The reduced graphene was filtered out with nylon membrane (0.45 mm), washed several times with water and dried under vacuum for 48 h at 60 °C.

The reduced G-HU-Control sample for comparison was prepared in a similar manner, with the exception of 2 g of sodium amide being used in place of elemental sodium.

Apparatus and Sample Preparation. Scanning electron micrographs (SEM) were obtained with a JEOL 7600F field-emission scanning electron microscope (JEOL, Japan) with a 2.0 kV acceleration voltage in gentle-beam mode, while energy dispersive X-ray spectroscopy (EDS) was performed at 15.0 kV. All reduced graphite oxide samples were attached onto a sticky conductive carbon tape mounted on an aluminum stage.

The FT-IR measurement was performed on FTIR spectrometer NICOLET 6700 (Thermo Scientific). A diamond ATR crystal and DTGS detector were used for the measurements.

For electrical resistivity measurements of graphene materials, 40 mg of the powder material was first compressed into a capsule of 0.2 in. diameter under a pressure of 400 MPa for 30 s. The resistivity of the resulting capsule was measured by a 4-probe technique using the Van der Pauw[45] method. The resistivity measurements were then performed with Keithley 6220 current source and Agilent 34970A data acquisition/switch unit. The measuring current was set to 10 mA.

X-ray photoelectron spectroscopy (XPS) was performed with a Phoibos 100 spectrometer using a Magnesium X-ray radiation source (SPECS, Germany). A wide-scan survey of all elements was performed. Relative sensitivity factors were used in evaluating the carbon-to-oxygen (C/O) ratios from the survey spectra. Samples were compressed onto conductive carbon tapes attached on aluminum sample holders.

An inVia Raman microscope (Renishaw, England) was used for Raman spectroscopy in backscattering geometry with a CCD detector. A DPSS laser was used (532 nm, 50 mW) with 50x magnification objective. Instrument calibration was achieved with a silicon reference which gives a peak position at 520 cm^{-1} and a resolution of less than 1 cm^{-1}. Samples used for the measurement was dispersed in isopropyl alcohol (1 mg/mL) and dried on silicon wafer. To avoid radiation damage of studied material, the laser power used for measurement was in the range of 50 nW to 500 μW. For the low temperature measurement of Raman and photoluminescence spectra, a pulse tube close cycle optical cryostat with base temperature of 11 K was used. The sample was mounted on an *x-y-z* piezoelectric stage with Apiezon N and covered with CaF_2 window. In this instance, a 20× magnification long working distance objective was used.

The magnetic measurements were performed using SQUID magnetometer MPMS-5S. At temperatures of 5 and 300 K, the hysteresis loops were recorded between −10 and 10 kOe. In the same temperature range (5−300 K), the zero-field cooled (ZFC) and field- cooled (FC) susceptibilities were measured under an applied field of 1000 Oe.

Trace analysis of impurities was performed with an optical emission spectrometer SPECTRO Arcos (SPECTRO Analytical

Instruments, Germany) with radial observation of inductively coupled plasma (ICP-OES). The spectrometer features a Paschen-Runge optic mount. Spectra were measured in the range from 130 to 770 nm. For sample introduction, a Cyclonic spray chamber and a Modified Lichte nebulizer were used. The following ICP operating parameters were applied: generator power 1450 W, coolant flow 13 L/min, auxiliary flow 0.8 L/min, nebulizer flow 0.8 L/min, sample aspiration rate 2 mL/min. Calibration was achieved using commercially available multielement standard solutions (Analytika). The concentrations of all calibrated elements were 0, 0.1, 0.5, 2.0, and 10.0 mg/L, respectively. A total of 5 mg/L Y was used as an internal standard. All measurements were performed in 4% HNO_3 as a matrix. The detection limits for analyzed elements ranged about 1 ppb within the measured decomposed sample. To prepare liquid samples for ICP-OES analysis, the solid samples were weighed (approximately 5 mg) on microanalytical balance and combusted by the Schöniger method.[46] Afterward, the closed Erlenmeyer flask was treated in an ultrasonic bath. After absorption of combustion products (at least 2 h), 0.88 mL of concentrated HNO_3 (suprapure) and 100 μL of 1 mg/mL Y standard solution were added. The liquid mixture was quantitatively transferred from the glass flask to a plastic bottle, and made up to a final volume of 20 mL with weighing. Finally, the solution was filtered and introduced to the spectrometer system. The baseline of the ICP-OES measurements was subtracted from a blank experiment.

The impurities' concentration was also investigated by X-ray fluorescence spectrometer SPECTRO iQ II (SPECTRO Analytical Instruments, Germany) equipped with silicon drift detector. The instrument uses a polarized primary radiation for increased sensitivity and the noise reduction and all radiation paths are flushed with helium.

Combustible elemental analysis (CHNS-O) was performed with a PE 2400 Series II CHNS/O Analyzer (Perkin-Elmer). In CHN operating mode (the most robust and interference free mode), the instrument employs a classical combustion principle to convert the sample elements to simple gases (CO_2, H_2O and N_2). The PE 2400 analyzer performs automatically combustion and reduction, homogenization of product gases, separation and detection. A microbalance MX5 (Mettler Toledo) is used for precise weighing of samples (1.5−2.5 mg per single sample analysis). The accuracy of CHN determination is better than 0.30% abs. Internal calibration is performed using N-fenyl urea.

Conflict of Interest: The authors declare no competing financial interest.

Acknowledgment. M.P. thanks MINDEF/NTU fund JPP 11/02/637 06 and JSPS-NTU fund. Z.S. and F.Š. were supported by Specific University Research (MSMT No 20/2013) and Czech Science Foundation (project No. 13-20507S).

Supporting Information Available: FTIR spectra of materials illustrating C−H bond vibrations; tabulated elemental atomic composition values from energy-dispersive X-ray spectroscopy; EDS mappings of hydrogenated graphenes; elemental analysis (wt %) of hydrogenated graphenes based on combustible analysis; FT Raman spectra of hydrogenated graphenes; low temperature Raman spectroscopy of hydrogenated graphene (G-HO). This material is available free of charge *via* the Internet at http://pubs.acs.org.

REFERENCES AND NOTES

1. Sofo, J. O.; Chaudhari, A. S.; Barber, G. D. Graphane: A Two-Dimensional Hydrocarbon. *Phys. Rev. B* **2007**, *75*, 153401.
2. Samarakoon, D. K.; Wang, X. Chair and Twist-Boat Membranes in Hydrogenated Graphene. *ACS Nano* **2009**, *3*, 4017–4022.
3. Shkrebtii, A. I.; Heritage, E.; McNelles, P.; Cabellos, J. L.; Mendoza, B. S. Graphene and Graphane Functionalization with Hydrogen: Electronic and Optical Signatures. *Phys. Status Solidi C* **2012**, *9*, 1378–1383.
4. Lebègue, S.; Klintenberg, M.; Eriksson, O.; Katsnelson, M. I. Accurate Electronic Band Gap of Pure and Functionalized Graphane from GW Calculations. *Phys. Rev. B* **2009**, *79*, 245117.
5. AlZahrani, A. Z.; Srivastava, G. P. Structural and Electronic Properties of H-Passivated Graphene. *Appl. Surf. Sci.* **2010**, *256*, 5783–5788.
6. Lu, N.; Li, Z.; Yang, J. Electronic Structure Engineering *via* On-Plane Chemical Functionalization: A Comparison Study on Two Dimensional Polysilane and Graphane. *J. Phys. Chem. C* **2009**, *113*, 16741–16746.
7. Zhou, J.; Sun, Q. How to Fabricate a Semihydrogenated Graphene Sheet? A Promising Strategy Explored. *Appl. Phys. Lett.* **2012**, *101*, 073114.
8. Schäfer, R. A.; Englert, J. M.; Wehrfritz, P.; Bauer, W.; Hauke, F.; Seyller, T.; Hirsch, A. On the Way to Graphane-Pronounced Fluorescence of Polyhydrogenated Graphene. *Angew. Chem., Int. Ed.* **2013**, *52*, 754–757.
9. Zhou, J.; Wang, Q.; Sun, Q.; Chen, X. S.; Kawazoe, Y.; Jena, P. Ferromagnetism in Semihydrogenated Graphene Sheet. *Nano Lett.* **2009**, *9*, 3867–3870.
10. Elias, D. C.; Nair, R. R.; Mohiuddin, T. M. G.; Morozov, S. V.; Blake, P.; Halsall, M. P.; Ferrari, A. C.; Boukhvalov, D. W.; Katsnelson, M. I.; Geim, A. K.; *et al.* Control of Graphene's Properties by Reversible Hydrogenation: Evidence for Graphane. *Science* **2009**, *323*, 610–613.
11. Burgess, J. S.; Matis, B. R.; Robinson, J. T.; Bulat, F. A.; Perkins, F. K.; Houston, B. H.; Baldwin, J. W. Tuning the Electronic Properties of Graphene by Hydrogenation in a Plasma Enhanced Chemical Vapor Deposition Reactor. *Carbon* **2011**, *49*, 4420–4426.
12. Luo, Z.; Yu, T.; Kim, K.; You, Y.; Lim, S.; Shen, Z.; Wang, S.; Lin, J. Thickness-Dependent Reversible Hydrogenation of Graphene Layers. *ACS Nano* **2009**, *3*, 1781–1788.
13. Kim, H.; Balgar, T.; Hasselbrink, E. Is There sp^3-Bound H on Epitaxial Graphene? Evidence for Adsorption on Both Sides of the Sheet. *Chem. Phys. Lett.* **2012**, *546*, 12–17.
14. Xie, L.; Wang, X.; Lu, J.; Ni, Z.; Luo, Z.; Mao, H.; Wang, R.; Wang, Y.; Huang, H.; Qi, D.; *et al.* Room Temperature Ferromagnetism in Partially Hydrogenated Epitaxial Graphene. *Appl. Phys. Lett.* **2011**, *98*, 193113.
15. Poh, H. L.; Šaněk, F.; Sofer, Z.; Pumera, M. High-Pressure Hydrogenation of Graphene: Towards Graphane. *Nanoscale* **2012**, *4*, 7006–7011.
16. Subrahmanyam, K. S.; Kumar, P.; Maitra, U.; Govindaraj, A.; Hembram, K. P. S. S.; Waghmare, U. V.; Rao, C. N. R. Chemical Storage of Hydrogen in Few-Layer Graphene. *Proc. Natl. Acad. Sci. U.S.A.* **2011**, *108*, 2674–2677.
17. Yang, Z.; Sun, Y.; Alemany, L. B.; Narayanan, T. N.; Billups, W. E. Birch Reduction of Graphite. Edge and Interior Functionalization by Hydrogen. *J. Am. Chem. Soc.* **2012**, *134*, 18689–18694.
18. Sepioni, M.; Nair, R. R.; Narayanan, J.; Tuna, F.; Winpenny, R.; Geim, A. K.; Grigorieva, I. V. Limits on Intrinsic Magnetism in Graphene. *Phys. Rev. Lett.* **2010**, *105*, 207205.
19. Berashevich, J.; Charkraborty, T. Sustained Ferromagnetism Induced by H-Vacancies in Graphane. *Nanotechnology* **2010**, *21*, 355201.
20. Nair, R. R.; Sepioni, M.; Tsai, I.; Lehtinen, O.; Keinonen, J.; Krasheninnikov, A. V.; Thomson, T.; Geim, A. K.; Grigorieva, I. V. Spin-Half Paramagnetism in Graphene Induced by Point Defects. *Nat. Phys.* **2012**, *8*, 199–202.
21. Panich, M.; Shames, A. I.; Nakajima, T. On Paramagnetism in Fluorinated Graphite: EPR and Solid State NMR Study. *J. Phys. Chem. Solids* **2001**, *62*, 959–964.
22. Wang, Y.; Huang, Y.; Song, Y.; Zhang, X.; Ma, Y.; Liang, J.; Chen, Y. Room-Temperature Ferromagnetism of Graphene. *Nano Lett.* **2009**, *9*, 220–224.
23. Hong, J.; Bekyarova, E.; Liang, P.; Haddon, R. C.; Khizroev, S. Room-Temperature Magnetic Ordering in Functionalized Graphene. *Sci. Rep.* **2012**, *2*, 624.
24. McIntosh, R.; Mamo, M. A.; Jamieson, B.; Roy, S.; Bhattacharyya, S. Improved Electronic and Magnetic Properties of Reduced Graphene Oxide Films. *Europhys. Lett.* **2012**, *97*, 38001.
25. Santos, E. J. G.; Ayuela, A.; Sánchez-Portal, D. Universal Magnetic Properties of sp^3-Type Defects in Covalently Functionalized Graphene. *New J. Phys.* **2012**, *14*, 043022.
26. Fang, M.; Wang, K.; Lu, H.; Yang, Y.; Nutt, S. Covalent Polymer Functionalization of Graphene Nanosheets and

Mechanical Properties of Composites. *J. Mater. Chem.* **2009**, *19*, 7098–7105.
27. Dreyer, D. R.; Park, S.; Bielawski, C. W.; Ruoff, R. S. The Chemistry of Graphene Oxide. *Chem. Soc. Rev.* **2010**, *39*, 228–240.
28. Kumar, A.; Reddy, A. L. M.; Mukherjee, A.; Dubey, M.; Zhan, X.; Singh, N.; Ci, L.; Billups, W. E.; Nagurny, J.; Mital, G.; *et al.* Direct Synthesis of Lithium-Intercalated Graphene for Electrochemical Energy Storage Application. *ACS Nano* **2011**, *5*, 4345–4349.
29. Feng, H.; Cheng, R.; Zhao, X.; Duan, X.; Li, J. A Low-Temperature Method to Produce Highly Reduced Graphene Oxide. *Nat. Commun.* **2013**, *4*, 1539.
30. Staudenmaier, L. Verfahren zur Darstellung der Graphitsäure. *Ber. Dtsch. Chem. Ges.* **1898**, *31*, 1481–1487.
31. Hofmann, U.; Konig, E. Untersuchungen Uber Graphitoxyd. *Z. Anorg. Allg. Chem.* **1937**, *234*, 311–336.
32. Hummers, W. S.; Offeman, R. E. Preparation of Graphitic Oxide. *J. Am. Chem. Soc.* **1958**, *80*, 1339.
33. Birch, A. J. Reduction by Dissolving Metals. Part I. *J. Chem. Soc.* **1944**, 430–436.
34. Stoller, M. D.; Park, S.; Zhu, Y.; An, J.; Ruoff, R. S. Graphene-Based Ultracapacitors. *Nano Lett.* **2008**, *8*, 3498.
35. Yoon, C.-M.; Long, D.; Jang, S.-M.; Qiao, W.; Ling, L.; Miyawaki, J.; Rhee, C.-K.; Mochida, I.; Yoon, S.-H. Electrochemical Surface Oxidation of Carbon Nanofibers. *Carbon* **2011**, *49*, 96–105.
36. Ros, T. G.; van Dillen, A. J.; Geus, J. W.; Koningsberger, D. C. Surface Oxidation of Carbon Nanofibres. *Chem.—Eur. J.* **2002**, *8*, 1151–1162.
37. Gao, W.; Alemany, L. B.; Ci, L.; Ajayan, P. M. New Insights into the Structure and Reduction of Graphite Oxide. *Nat. Chem.* **2009**, *1*, 403–408.
38. Okpalugo, T. I. T.; Papakonstantinou, P.; Murphy, H.; McLaughlin, J.; Brown, N. M. D. High Resolution XPS Characterization of Chemical Functionalised MWCNTs and SWCNTs. *Carbon* **2005**, *43*, 153.
39. Chua, C. K.; Sofer, Z.; Pumera, M. Graphite Oxides: Effects of Permanganate and Chlorate Oxidants on the Oxygen Composition. *Chem.—Eur. J.* **2012**, *18*, 13453–13459.
40. Cançado, L. G.; Takai, K.; Enoki, T.; Endo, M.; Kim, Y. A.; Mizusaki, H.; Jorio, A.; Coelho, L. N.; Magalhães-Paniago, R.; Pimenta, M. A. General Equation for the Determination of the Crystallite Size L_a of Nanographite by Raman Spectroscopy. *Appl. Phys. Lett.* **2006**, *88*, 163106.
41. Gao, H.; Wang, L.; Zhao, J.; Ding, F.; Lu, J. Band Gap Tuning of Hydrogenated Graphene: H Coverage and Configuration Dependence. *J. Phys. Chem. C* **2011**, *115*, 3236–3242.
42. Heremans, J.; Olk, C. H.; Moreli, D. T. Magnetic Susceptibility of Carbon Structures. *Phys. Rev. B* **1994**, *49*, 15122.
43. Esquinazi, P.; Setzer, A.; Höhne, R.; Semmelhack, C.; Kopelevich, Y.; Spemann, D.; Butz, T.; Kohlstrunk, B.; Löshce, M. Ferromagnetism in Oriented Graphite Samples. *Phys. Rev. B* **2002**, *66*, 024429.
44. Yazyev, O. V.; Helm, L. Defect-Induced Magnetism in Graphene. *Phys. Rev. B* **2007**, *75*, 12540.
45. Van der Pauw, L. J. A Method of Measuring Specific Resistivity and Hall Effect of Discs of Arbitrary Shape. *Philips Res. Rep.* **1958**, *13*, 1–9.
46. Schöniger, W. Eine Mikroanalytische Schnellbestimmung von Halogen in Organischen Substanzen. *Microchim. Acta* **1955**, *43*, 123–129.